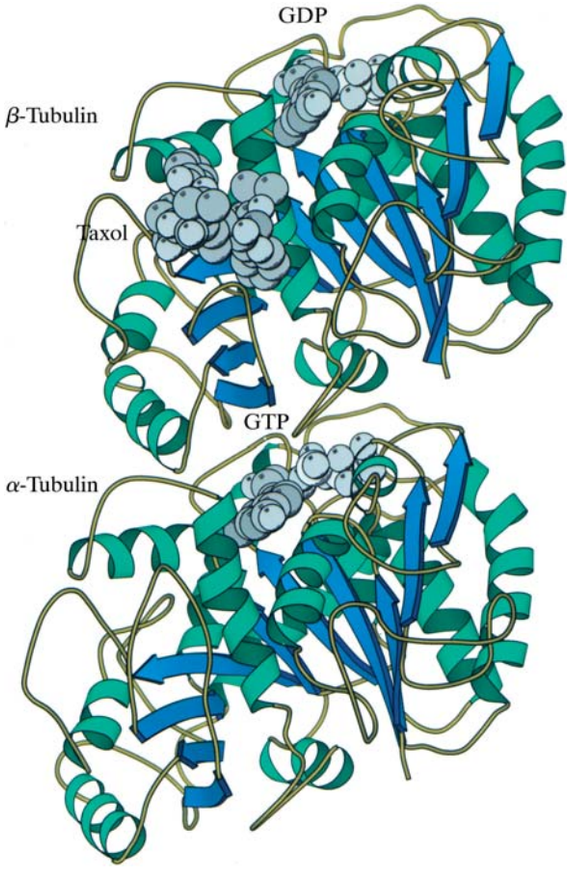

Fig. 19.2.4.3. Ribbon diagram of a tubulin dimer, whose structure has been solved to 3.7 Å resolution. GTP, GDP and taxol are shown as CPK models, with GDP at the top, bound to β tubulin, and GTP in the middle, bound to the α subunit. This is the view as seen from inside a microtubule, with the plus end at the top. (Courtesy of Drs Eva Nogales and Kenneth Downing at the Lawrence Berkeley National Laboratory, University of California, Berkeley.)

required accuracy of these angular determinations depends on the thickness of the crystal and also on the desired resolution (Prasad *et al.*, 1990). For instance, the angular accuracy has to be $<0.1^\circ$ for 3.5 Å data in a 100 Å-thick crystal. The sampling of the data along the lattice line is generally about $\frac{1}{4}$ the thickness of the crystal (Henderson *et al.*, 1990). The data points are not evenly sampled along the lattice lines; they must be fitted into continuous and smoothly varying functions within the constraint of the crystal thickness. These functions are interpolated onto a periodic lattice, so that its inverse Fourier transform can be computed to reconstruct the three-dimensional mass-density function of the object.

19.2.4.2. *Amplitudes and phases*

An electron-microscope image contains both the amplitudes and phases of the structure factors. The basic premise of the current image-reconstruction scheme assumes that the image intensity can be related to the structure factor linearly and can be retrieved by the Fourier transform of the image intensities. However, the structure factors, $F(S)$, are influenced by several instrumental factors, as shown in equations (19.2.4.1)–(19.2.4.3) below, whose parameters need to be determined for each image.

$$F^2_{\rm obs}(S) = [F(S){\rm CTF}(S)E(S)]^2 + N^2(S), \quad (19.2.4.1)$$

$${\rm CTF}(S) = -\{(1-Q^2)^{1/2}\sin[\gamma(S)] + Q\cos[\gamma(S)]\} \text{ and} \quad (19.2.4.2)$$

$$\gamma(S) = \pi[(-C_s\lambda^3 S^4)/2 + \Delta z \lambda S^2], \quad (19.2.4.3)$$

where $F_{\rm obs}$ is the structure factor computed from the electron cryomicroscopic images, F is the true structure factor, CTF is the contrast-transfer function, E is the product of many decay functions due to the electron optics and specimen movement, N is the background noise contributed by a variety of physcial effects, S is the spatial frequency, Q is the fraction of amplitude contrast, C_s is the spherical aberration coefficient of the objective lens, λ is the wavelength and Δz is the image defocus.

In practice, it is tedious to determine all the parameters in these equations from images in order to make corrections to the amplitudes of the structure factors. In the case of crystals, the amplitudes of the structure factors can simply be obtained directly from the electron diffraction intensities, which are free from any of the above factors (Unwin & Henderson, 1975). The computational procedure used to calculate the diffraction spot intensities is similar to that used to measure an X-ray diffraction pattern (Baldwin & Henderson, 1984; Brink & Wei Tam, 1996). The quality of the diffraction intensity measurement is evaluated from the value of $R_{\rm sym}$ for Friedel-related reflections. The best data have $R_{\rm sym}$ less than 0.04. The consistency of the diffraction intensities among different patterns from different crystals is judged from $R_{\rm merge}$, which is generally 0.15–0.25 (Kimura *et al.*, 1997; Nogales *et al.*, 1998). Fig. 19.2.4.2 is an example of the diffraction intensity for two lattice lines computed from bacteriorhodopsin crystals. The phases of the structure factors are computed from images.

In addition to the instrumental factors given in equations (19.2.4.1)–(19.2.4.3), however, images are generally imperfect because of bending of the crystal, specimen preparation, or magnification variations across an image. The consequence of these imperfections is a reduction of the signal-to-noise ratio in high-resolution reflections. A computational procedure called 'unbending' has been devised, which in effect fixes the image imperfection by finding the unit-cell deviation vectors and straightening them by interpolation (Henderson *et al.*, 1986). The effect of the instrumental factors is the modulation of the phases by the oscillating function CTF(S), as shown in equations (19.2.4.1)–(19.2.4.3). The result is that the phases flip by π at different frequencies, depending on the defocus setting (Erickson & Klug, 1970). In addition, there is a phase shift caused by a combination of factors, including lens astigmatism, beam tilt and specimen height variation in a tilted position. All of these factors have to be corrected for each micrograph before merging the phases of the reflections from different micrographs to a common phase origin. The determination of the phase origin is performed by phase residual difference minimization or correlation matches among different micrographs (Amos *et al.*, 1982; Thomas & Schmid, 1995). Intensities and corresponding phases of two lattice lines are shown in Fig. 19.2.4.2. The fitted curves show the matches among the data points, each of which is from a different image or from different symmetry-related reflections from the same image.

In electron crystallography, the correctness of the phases can be evaluated by the self-consistency of the merged data sets and also by the phase residual difference of the symmetry-related reflections according to the two-dimensional plane-group symmetry. For two-dimensional crystals, there are only 17 possible plane groups (Amos *et al.*, 1982). As in the case of a three-dimensional crystal, the plane group is determined from the symmetry of the phases, the unit-cell parameters and the pattern of forbidden reflections. The plane-group assignment can be confirmed by the phase equivalence of symmetry-related reflections. Furthermore, the reliability of the

map can be judged by the figure of merit of the phases, computed from the phase probability distribution function of the observed reflections.

19.2.4.3. *3D map*

The three-dimensional (3D) map is computed from the amplitudes and phases at the resolution defined by the data (Henderson & Unwin, 1975). The resolution reported for the structure is defined by the observed reflections in the images. Owing to the missing data at high tilt angles, the reconstruction normally has a lower resolution in the direction of the electron beam than in the direction normal to it. As a result, many of the initial low-resolution structures appear stretched out along the vertical direction. The interpretation of the 3D map derived from electron crystallography is similar to that of X-ray crystallography. Often, the initial map is reported at about 7 Å, where some of the α-helices can be interpreted. With an improved map of about 3.5 Å, the polypeptide backbone is traced and some of the bulky side chains are recognized. Fig. 19.2.4.3 shows a chain tracing of a tubulin crystal (Nogales *et al.*, 1998).

19.2.4.4. *Refinement*

In order to arrive at a correct mechanistic model for the protein, an accurate atomic structure is needed. So far, in electron crystallography only bacteriorhodopsin has been refined (Grigorieff *et al.*, 1996). A common criterion used in X-ray crystallography to evaluate the progress of refinement is based on the free *R* factor, which measures the agreement between the model and a part of the experimental data not included in the refinement process. In electron crystallography, the phases are measured independently from images and hence are not refined. Therefore, they can be used as a 'free phase residual,' which is analogous to the free *R* factor, to assess the progress of refinement. The refined structure would result in improved peptide geometry, increased accuracy of the coordinates of the polypeptide backbone and of the amino-acid side chain residues, and improved temperature factors of the residues.

19.2.5. Future development

Electron crystallography has proven to be a high-resolution structural tool for two-dimensional protein crystals, to the point where the polypeptide backbone can be traced and atomic coordinates derived. Needless to say, there is still much to be learned about how to make highly ordered two-dimensional crystals from either membrane or soluble proteins. Research in this direction is critical for the growth of electron crystallography. Recent results have promoted optimism; there has been an increase in the number of membrane proteins crystallized into two-dimensional arrays from which at least 6 to 8 Å structures can be obtained (Walz *et al.*, 1997; Auer *et al.*, 1998; Zhang *et al.*, 1998; Unger *et al.*, 1999).

In the most recent high-resolution structural study of tubulin, a 3.7 Å map was obtained from 100 electron diffraction patterns and 150 electron images. Effectively, this structure was the result of a computational average of about one million tubulin dimers. It took six years to determine the structure from the time when the first high-resolution crystal structure was reported (Downing & Jontes, 1992; Nogales *et al.*, 1998). All the experimental and computational procedures were basically the same as those developed for bacteriorhodopsin (Henderson *et al.*, 1990). An obvious future development in protein electron crystallography would be aimed at improving the throughput of the structural determination. This entails a search for better solutions to some of the technical problems mentioned above as well as the introduction of automation in both data collection and processing.

Finally, another potentially exciting aspect of electron crystallography is the ability to detect charged residues from the high scattering differences between neutral and charged atoms. This physical property may make electron crystallography a unique method for detecting the ionization state of the amino-acid residues in proteins (Mitsuoka *et al.*, 1999). Furthermore, there is also a good prospect of extending the structure close to 2 Å resolution, as the next generation of electron cryomicroscope will be equipped with a field emission gun operated at 300 keV, a liquid helium cryo-specimen stage and an energy filter. This combination of instrumental features is likely to bring electron crystallography a step closer to its ultimate potential for structural biology research at the atomic level.

Acknowledgements

Research has been supported by RR002250. I thank Drs Jacob Brink, Michael Schmid, Karou Mitsuoka and Ken Downing for helpful comments on the manuscript.

references